Title

Equilibrium and kinetic models for colloid release under transient solution chemistry conditions

Authors

Bradford, Scott A
Torkzaban, Saeed
Leij, Feike
et al.

Publication Date

2015-10-01

DOI

10.1016/j.jconhyd.2015.04.003

Peer reviewed

Journal of Contaminant Hydrology 181 (2015) 141–152

Contents lists available at ScienceDirect

Journal of Contaminant Hydrology

journal homepage: www.elsevier.com/locate/jconhyd

Equilibrium and kinetic models for colloid release under transient solution chemistry conditions

Scott A. Bradford [a,*], Saeed Torkzaban [b], Feike Leij [c], Jiri Simunek [d]

[a] US Salinity Laboratory, USDA, ARS, Riverside, CA, United States
[b] CSIRO Land and Water, Glen Osmond, SA 5064, Australia
[c] Department of Civil Engineering and Construction Engineering Management, California State University, Long Beach, CA 90840-5101, United States
[d] Department of Environmental Sciences, University of California, Riverside, CA 92521, United States

ARTICLE INFO

Article history:
Received 3 December 2014
Received in revised form 26 March 2015
Accepted 8 April 2015
Available online 17 April 2015

Keywords:
Colloid
Microorganism
Model
Transients
Chemistry

ABSTRACT

We present continuum models to describe colloid release in the subsurface during transient physicochemical conditions. Our modeling approach relates the amount of colloid release to changes in the fraction of the solid surface area that contributes to retention. Equilibrium, kinetic, equilibrium and kinetic, and two-site kinetic models were developed to describe various rates of colloid release. These models were subsequently applied to experimental colloid release datasets to investigate the influence of variations in ionic strength (IS), pH, cation exchange, colloid size, and water velocity on release. Various combinations of equilibrium and/or kinetic release models were needed to describe the experimental data depending on the transient conditions and colloid type. Release of *Escherichia coli* D21g was promoted by a decrease in solution IS and an increase in pH, similar to expected trends for a reduction in the secondary minimum and nanoscale chemical heterogeneity. The retention and release of 20 nm carboxyl modified latex nanoparticles (NPs) were demonstrated to be more sensitive to the presence of Ca^{2+} than D21g. Specifically, retention of NPs was greater than D21g in the presence of 2 mM $CaCl_2$ solution, and release of NPs only occurred after exchange of Ca^{2+} by Na^{+} and then a reduction in the solution IS. These findings highlight the limitations of conventional interaction energy calculations to describe colloid retention and release, and point to the need to consider other interactions (e.g., Born, steric, and/or hydration forces) and/or nanoscale heterogeneity. Temporal changes in the water velocity did not have a large influence on the release of D21g for the examined conditions. This insensitivity was likely due to factors that reduce the applied hydrodynamic torque and/or increase the resisting adhesive torque; e.g., macroscopic roughness and grain–grain contacts. Our analysis and models improve our understanding and ability to describe the amounts and rates of colloid release and indicate that episodic colloid transport is expected under transient physicochemical conditions.

Published by Elsevier B.V.

1. Introduction

An understanding of and an ability to accurately predict the release of colloids (including microorganisms, particulate organic matter, clay, metal oxides, and nanoparticles) in porous media are needed for many agricultural, environmental, and industrial applications. Under steady-state flow and solution chemistry conditions low amounts of colloids are slowly released from the solid phase when the kinetic energy of diffusing colloids exceeds the adhesive interaction energy (Ryan and Elimelech, 1996; Ryan and Gschwend, 1994; Shen et al., 2007). Conversely, significant amounts of colloid release may rapidly occur during temporal changes (i.e., transients) in solution chemistry (Grolimund et al., 2001; Roy and Dzombak, 1996) and/or water velocity (Bergendahl and Grasso, 1998,

* Corresponding author. Tel.:+1 951 369 4857.
E-mail address: Scott.Bradford@ars.usda.gov (S.A. Bradford).

http://dx.doi.org/10.1016/j.jconhyd.2015.04.003
0169-7722/Published by Elsevier B.V.

2000). These observations indicate that different mechanisms control colloid release during steady-state and transient conditions. Transient physicochemical conditions may occur in the subsurface as a result of infiltration and recharge, groundwater and surface water interactions, injection and/or extraction wells, and contamination events.

Colloid immobilization and release at a particular location on the collector surface depend on the strength of the resisting adhesive torque in comparison to the applied hydrodynamic torque (Bergendahl and Grasso, 1998, 2000), and the adhesive interaction energy relative to the kinetic energy of diffusing colloids (Shen et al., 2007; Simoni et al., 1998). Transients in water velocity alter the hydrodynamic force that acts on immobilized colloids (Bergendahl and Grasso, 1998, 2000), and is spatially variable because of the complex geometry of the pore space (Bradford et al., 2011). Transient solution chemistry conditions impact the adhesive force by altering the macroscopic zeta potentials and the electric double layer thickness (Grolimund and Borkovec, 2006; Ryan and Elimelech, 1996). In addition, the dependence of the adhesive force on solution ionic strength (IS) is a function of the colloid size and the nanoscale heterogeneity (e.g., the distribution of charge and roughness) within the zone of electrostatic influence (Bendersky and Davis, 2011; Duffadar and Davis, 2007). Natural colloid and solid surfaces always exhibit some degree of nanoscale heterogeneity due to surface roughness, mineral defects, isomorphic substitution, protonation/deprotonation of hydroxyl groups, and adsorption of different ions, organics, and clay particles (Suresh and Walz, 1996; Tufenkji and Elimelech, 2005; Vaidyanathan and Tien, 1991). Consequently, spatial variability of the adhesive force is also expected. The above information indicates that transient physicochemical conditions initiate colloid release by altering the force and/or torque balance that acts on immobilized colloids, and that only a fraction of the retained colloids may be released because of spatial variations in the adhesive and hydrodynamic forces and torques.

Several continuum models have been developed to simulate colloid release during transients in solution chemistry (Bedrikovetsky et al., 2011; Bradford et al., 2012; Grolimund and Borkovec, 2006; Lenhart and Saiers, 2003; Tosco et al., 2009). In general, colloid transport equations are coupled to the solution chemistry through explicit dependencies of retention and/or release parameters on solute concentrations (e.g., IS, pH and/or adsorbed divalent cations). The transport equations for solution chemistry and colloids are subsequently solved and colloid transport parameters are updated at each time step. All of the continuum models employ different first-order kinetic formulations for colloid retention and release; e.g., some considered population heterogeneity, blocking, or multiple retention sites. In addition, the functional dependency of retention and release parameters on solution chemistry varies significantly among the models. Only some of these models can be easily extended to describe colloid release with transients in water velocity (Bedrikovetsky et al., 2011; Bradford et al., 2012).

One challenge in continuum modeling of colloid release is determining the amount of colloid release with the physicochemical perturbation. A finite number of colloids can be retained in porous media under steady-state conditions. The maximum solid phase concentration of retained colloids (S_{max}) is obtained when all retention sites are filled. Under steady-state conditions, the value of S_{max} can be determined by direct microscopic observations in simplified systems (Adamczyk et al., 1992), inverse optimization of experimental breakthrough curve data that exhibit blocking behavior (Adamczyk et al., 1994; Johnson and Elimelech, 1995), or theoretically estimated from torque balance calculations (Bradford et al., 2013). Experimental and theoretical results demonstrate that S_{max} is sensitive to the solution chemistry and hydrodynamic conditions (Adamczyk et al., 1995; Bradford et al., 2013; Sasidharan et al., 2014). Such changes in S_{max} with physicochemical conditions have been related to the amount of colloid release during transient conditions (Bedrikovetsky et al., 2011; Bradford et al., 2012). However, the dependence of S_{max} on physicochemical conditions is more complicated during colloid release than retention because some of the retained colloids cannot be released by a given perturbation (e.g., irreversible retention) (Adamczyk et al., 1992). The functional dependence of S_{max} on IS therefore exhibits hysteresis during retention and release phases (Bradford et al., 2012). The importance of temporal changes in S_{max} with transient conditions on colloid release is not widely appreciated, and has not yet been incorporated into continuum models that account for the full range of equilibrium and/or kinetic release behavior.

A second challenge in continuum modeling of colloid release with transient physicochemical conditions is describing the dynamics of colloid release. The adhesive interaction at a particular location on the collector surface may change with a physicochemical perturbation as ions transfer and/or react in the gap separating the colloid from the collector surface. Spatial variations in the adhesive (and associated separation distances) and hydrodynamic forces produce a distribution of mass transfer and reaction rates for ions on collector surfaces. Indeed, various combinations of equilibrium or kinetic models are needed to describe geochemical reactions of specific ions in soils (Mayer et al., 2002; Šimůnek and Valocchi, 2002). Similarly, colloid release with transients has sometimes been observed to occur slowly and at other times very rapidly (Bedrikovetsky et al., 2011; Bradford et al., 2012; Grolimund and Borkovec, 2006; Khilar and Fogler, 1984; Lenhart and Saiers, 2003; Shen et al., 2012; Torkzaban et al., 2013; Tosco et al., 2009). It is therefore logical to anticipate that equilibrium, kinetic, combined equilibrium and kinetic, or even two-site kinetic models may be needed to describe colloid release under transient physicochemical conditions. However, continuum models for colloid release have not yet been developed to describe all of these possible conditions.

The overall objective of this research is to improve our understanding of and ability to simulate colloid release under transient physicochemical conditions. This aim is accomplished by relating the amount of colloid release with transients to changes in S_{max}, and then developing equilibrium, kinetic, combined equilibrium and kinetic, and two-site kinetic models to describe a wide variety of observed colloid release behavior. These continuum models were subsequently applied to experimental colloid release datasets under various transient conditions to investigate the influence of IS, pH, cation exchange, colloid size, and water velocity on release. Analysis of these data improves our knowledge of fundamental factors influencing colloid release during transient physicochemical conditions, and helps to identify the proper model formulations to describe such behavior.

2. Materials and methods

2.1. Electrolyte solutions and porous medium

Electrolyte solutions were prepared using deionized (DI) water (pH = 5.8), and NaCl (0, 1, 5, 25, 50, and 100 mM NaCl) or $CaCl_2$ (2 mM $CaCl_2$) salts. Sodium bicarbonate and carbonate salts were added to the 100 mM NaCl solution to buffer the pH at values of 7, 8, 9, and 10 (Delory and King, 1945; Waentig et al., 2009). Ultrapure quartz sand (Iota Quartz, Unimin Corp. NC) was employed as porous medium in the transport and release experiments discussed below. The sand was thoroughly rinsed with DI water to eliminate background fines from the sand before use. The median grain size of this sand was measured to be 238 μm (standard deviation of 124 μm) with a laser scattering particle size and distribution analyzer (Horiba LA 930).

2.2. Colloids

Experiments discussed below employed pure cultures of *Escherichia coli* D21g or carboxyl modified latex (CML) nanoparticles (NPs). D21g is a gram-negative, nonmotile bacterial strain that produces minimal amounts of lipopolysaccharides and extra-cellular polymeric substances. *E. coli* D21g was grown 24 h before initiating experiments. A single colony of *E. coli* D21g was inoculated into 1.0 l of Luria-Bertani media containing 30 mg/L gentamycin and incubated with shaking at 37 °C overnight. The bacterial suspension was centrifuged and rinsed three times before diluting the concentrated suspension into the desired electrolyte solution. Influent and effluent concentrations of *E. coli* D21g were determined using a spectrophotometer (Unico UV-2000, United Products & Instruments, Dayton, NJ) at a wavelength of 600 nm and a calibration curve. The average optical density at 600 nm for the influent cell suspension was about 0.2, which corresponds to an input concentration (C_o) of approximately 10^7 CFU ml^{-1}. The size of *E. coli* D21g in the various solution chemistries was measured using the laser scattering particle size and distribution analyzer to be 1.46 μm.

The CML NPs (Molecular Probes, Eugene, OR) were fluorescent with excitation at 505 nm and emission at 515 nm. The manufacturer provided values of the CML NP size (20 nm in diameter), shape (spherical), density (1.05 g cm^{-3}), and hydrophobicity (hydrophilic). The stock CML NP solution was diluted to achieve a value of $C_o = 5 * 10^7$ N ml^{-1} for transport experiments. Average (three measurements) CML NP concentrations reported herein were determined using a Turner Quantech Fluorometer (Barnstead/Thermolyne, Dubuque, IA) and reproducibility was typically within 1% of C_o.

2.3. Interaction energy calculations

The zeta potential of *E. coli* D21g, CML NPs, and crushed ultrapure quartz sand in the various solution chemistries was determined from measured electrophoretic mobilities using a ZetaPALs instrument (Brookhaven Instruments Corporation, Holtsville, NY) and the Smoluchowski equation. The total interaction energy of *E. coli* D21 g and CML NP upon approach to the quartz sand under the various solution chemistries was calculated using Derjaguin–Landau–Verwey–Overbeek (DLVO) theory and a sphere–plate assumption (Derjaguin and Landau, 1941; Verwey and Overbeek, 1948). Electrostatic double layer interactions were quantified using the expression of Hogg et al. (1966). As is commonly assumed, zeta potentials were used in place of surface potentials in these calculations (Elimelech et al., 1995). The retarded London–van der Waals attractive interaction force was determined from the expression of Gregory (1981). The Hamaker constant was $6.5 * 10^{-21}$ J for D21g (Rijnaarts et al., 1995) and $4.04 * 10^{-21}$ J for CML NPs (Bergendahl and Grasso, 1999). Table 1 summarizes measured values for zeta potentials for D21g, CML NPs, and sand, and the calculated energy barrier height and depth of the secondary minimum for the DLVO interaction energies in the various solution chemistries.

It should be mentioned that DLVO theory is based on a number of assumptions (in addition to those noted above) that may be violated. For example, non-DLVO interaction energies such as Born repulsion, steric interactions, hydrophobic interactions, and/or hydration effects frequently need to be included in interaction energy calculations to explain experimental observations (Elimelech et al., 1995). Furthermore, conventional DLVO calculations employ mean values of zeta potentials and implicitly assume geometrically smooth and chemically homogeneous surfaces (Bendersky and Davis, 2011; Duffadar and Davis, 2007; Shen et al., 2012). However, natural colloid and solid surfaces always exhibit some degree of nanoscale heterogeneity. Consequently, the above DLVO calculations should therefore be viewed as only a first approximation of expected changes in mean adhesion with solution chemistry.

2.4. Column experiments

Glass chromatography columns (15 cm long and 4.8 cm inside diameter) were wet packed with the ultrapure quartz sand. The saturated water content, bulk density, and length for the packed column were determined to be about 0.44 cm^3 cm^{-3}, 1.48 g cm^{-3}, and 12.8 cm (adjustable fitting at the column top), respectively. Colloid retention in the sand was achieved by pumping six pore volumes (PVs) of a selected suspension upward through the vertically oriented columns at a steady flow rate using a peristaltic pump (Phase 1), followed by continued flushing with colloid free solution having the same solution chemistry for an additional 4 PVs (Phase 2). Colloid release was then studied by systematically changing the chemistry or velocity of the eluting solution (Phase 3) for 4–6 PVs at each alteration step. Specific experiments and justification for the selected physicochemical sequence are provided below. Effluent samples were continuously collected during the transport experiment at selected intervals using a fraction collector. The effluent samples were then analyzed for D21g or CML NPs as described above. Experiments were typically replicated and exhibited good reproducibility.

The influence of IS reduction on D21g release was studied using the following solution chemistry sequence: 100 (Phases 1 and 2), 50 (Phase 3a), 25 (Phase 3b), 5 (Phase 3c), 1 (Phase 3d), and 0 (Phase 3e) mM NaCl when the solution pH = 5.8 and the Darcy water velocity (q_w) equals 0.27 cm min^{-1}. This solution chemistry sequence was selected to encompass a range in mean adhesive interactions that ranged from favorable to progressively more unfavorable for D21g attachment (Table 1).

The effects of pH increase in 100 mM NaCl solution on D21g release was studied when q_w = 0.27 cm min^{-1} using the

Table 1
Zeta potentials and DLVO interaction energy parameters. The standard error associated with the zeta potentials is given in the parenthesis.

Colloid	NaCl or $CaCl_2$ (mM)	pH	Sand zeta potential (mV)	Colloid zeta potential (mV)	Energy barrier (kT)	Secondary energy minimum (kT)
D21g	1	5.8	−66.8 (3.0)	−57.2 (1.3)	3579.8	0.0
D21g	5	5.8	−63.3 (2.4)	−54.6 (1.5)	2892.2	−0.4
D21g	25	5.8	−57.2 (1.0)	−41.4 (1.4)	1453.1	−2.8
D21g	50	5.8	−41.4 (1.9)	−32.3 (1.1)	600.7	−6.7
D21g	100	5.8	−17.3 (1.8)	−17.5 (2.3)	NB	–
D21g	100	7.0	−21.0 (7.1)	−16.2 (2.6)	NB	–
D21g	100	8.0	−37.0 (4.9)	−16.2 (3.1)	56.2	−23.3
D21g	100	9.0	−38.9 (2.4)	−26.4 (6.4)	214.1	−19.6
D21g	100	10.0	−37.2 (3.1)	−18.9 (1.6)	49.2	−30.1
NP	1	5.8	−66.8 (3.0)	−34.1 (2.4)	22.1	0.0
NP	100	5.8	−17.3 (1.8)	−28.1 (8.9)	1.5	−0.1
D21g*	2	5.8	−28.6 (0.9)	−24.8 (0.5)	465.9	−0.8
NP*	2	5.8	−28.6 (0.9)	−14.9 (0.9)	3.2	0.0

NP — Carboxyl modified latex nanoparticle (20 nm in diameter).
NB — no barrier to attachment.
kT — product of the Boltzmann's constant and the absolute temperature.
* — $CaCl_2$ solution.

following solution chemistry sequence: pH = 5.8 (Phases 1 and 2), pH = 7 (Phase 3a), pH = 8 (Phase 3b), pH = 9 (Phase 3c), and pH = 10 (Phase 3d). Increases in solution pH can cause deprotonation of surface hydroxyl groups that may decrease the charge of nanoscale chemical heterogeneity sites (Tufenkji and Elimelech, 2005; Vaidyanathan and Tien, 1991). The solution IS also increased with pH because of the addition of various amounts of buffering salts (sodium bicarbonate and carbonate salts). The 100 mM NaCl solution and buffer produced conditions that were mainly favorable for attachment based on mean zeta potentials (Table 1), but that neglect the potential effects of nanoscale chemical heterogeneity. This solution chemistry sequence was therefore chosen to study the effects of changes in nanoscale chemical heterogeneity on D21g release.

Another experiment examined the influence of q_w on the release of D21g. In this case, D21g was deposited in 100 mM NaCl at pH 5.8 and $q_w = 0.27$ cm min^{-1} (Phases 1 and 2), and then the IS was reduced to 5 mM NaCl at pH = 5.8 (Phase 3). The value of q_w was then sequentially increased during Phase 3 using the following sequence: 0.27 (Phase 3a), 0.54 (Phase 3b), 1.08 (Phase 3c), 2.16 (Phase 3d), and 5.4 (Phase 3e) cm min^{-1}. The solution IS was chosen to be initially high (100 mM NaCl) in order to achieve similar initial conditions to the IS and pH release experiments discussed above. The solution was subsequently lowered to 5 mM NaCl in order to reduce the adhesive interaction (Table 1) and thereby facilitate release with changes in water velocity. Increases in water velocity were expected to initiate release by increasing the hydrodynamic force on immobilized D21g.

The influence of cation type and IS (pH = 5.8) on the release of D21g and CML NPs was investigated using the following solution chemistry sequence: 2 mM $CaCl_2$ solution (Phases 1 and 2), DI water (Phase 3a), 100 mM NaCl (Phase 3b), and DI water (Phase 3c) when the pH = 5.8 and $q_w = 0.27$ cm min^{-1}. Adsorbed multivalent cations, such as Ca^{2+}, can create nanoscale chemical heterogeneity on the solid surface that can neutralize or reverse the surface charge at specific locations (Grosberg et al., 2002). The initial solution composition was therefore selected to be 2 mM $CaCl_2$ in order to study the effects of a nanoscale chemical heterogeneity arising from the adsorption of Ca^{2+} on colloid retention and release. The mean adhesive interaction was dramatically reduced in the presence of DI water during Phases 3a and 3c (Table 1). Cation exchange (Ca^{2+} is exchanged by Na^{+}) may be initiated when 100 mM NaCl is added during (Phase 3b), and this may alter the amount of nanoscale chemical heterogeneity arising for adsorbed Ca^{2+}. The second DI water pulse (Phase 3c) was conducted to observe differences in release following alteration of the nanoscale heterogeneity by cation exchange. Two colloid sizes (20 nm CML colloids and 1.46 μm D21g) were considered because the effects of nanoscale chemical heterogeneity on the local adhesive interaction are known to be a function of the colloid size (Bendersky and Davis, 2011; Duffadar and Davis, 2007). Ideally, both colloids would have the same surface properties. However, the literature indicates that even the surface properties of CML colloids vary with size (Bradford and Kim, 2012; Treumann et al., 2014). Trends for D21g retention, release, and surface properties have been observed to be generally consistent with 1 μm CML colloids (Bradford and Kim, 2012; Bradford et al., 2012). Consequently, D21g was used as the larger colloid to be consistent with other release studies discussed above.

3. Continuum model development

Continuum scale models for colloid transport, retention and release are described below. These models were implemented into the Hydrus-1D (Šimůnek et al., 2008) software package. Details of the numerical solution and iterative procedure for nonlinear flow and transport problems are already presented in the literature (Šimůnek et al., 2008). Hydrus-1D includes a nonlinear least squares routine for inverse parameter optimization.

3.1. Steady-state colloid retention and release

Colloid transport in the aqueous phase was described using the advection–dispersion equation that includes an exchange term to/from the aqueous and the solid phases:

$$\frac{\partial \theta_w C}{\partial t} + \rho_b \frac{\partial S}{\partial t} = \frac{\partial}{\partial z}\left(\theta_w D \frac{\partial C}{\partial z}\right) - \frac{\partial q_w C}{\partial z} \quad (1)$$

where C [NL^{-3}; where N and L denote units of number and length, respectively] is the colloid concentration in the aqueous phase, D [L^2T^{-1}; where T denotes units of time] is the hydrodynamic dispersion coefficient for colloids, θ_w [L^3L^{-3}] is the volumetric water content, ρ_b [$M\ L^{-3}$; where M denotes units of mass] is the soil bulk density, and S [$N\ M^{-1}$] is the solid phase colloid concentration. The first and second terms on the right hand side of Eq. (1) account for the dispersive and advective fluxes of the colloids, respectively.

The solid phase mass balance equation during steady-state physicochemical conditions (e.g., Phases 1 and 2) is given in this work as:

$$\rho_b \frac{\partial S}{\partial t} = \theta \psi k_{sw} C - \rho_b k_{rs} S \tag{2}$$

where k_{sw} [T^{-1}] is the retention rate coefficient, k_{rs} [T^{-1}] is the steady-state release rate coefficient, and ψ [−] is a dimensionless blocking function. The parameter ψ accounts for time and concentration dependent blocking using a Langmuirian approach as (Adamczyk et al., 1994):

$$\psi = 1 - \frac{S}{S_{\max}} \tag{3}$$

3.2. Amount of transient colloid release

A first step in modeling colloid release with transient physicochemical conditions is determining the amount of colloid release with a given perturbation. Fig. 1 presents an illustration of the hypothetical fraction of the solid surface area that contributes to colloid immobilization (A_f) for two spherical collectors after equilibrating with three IS conditions (10, 50, and 100 mM). The value of A_f increases with the IS because of an increase in the depth of the secondary minimum and/or an increasing influence of nanoscale heterogeneities (Bendersky and Davis, 2011; Tufenkji and Elimelech, 2005). There is a linear relationship between A_f and S_{max} that is given as (Bradford et al., 2009):

$$S_{\max} = \frac{(1-\gamma) A_s A_f}{A_c \rho_b} \tag{4}$$

where A_c [$L^2\ N^{-1}$] is the cross-sectional area per colloid, A_s [L^{-1}] is the solid surface area per unit volume, and γ [−] is the porosity of a monolayer packing of colloids on the solid surface (a value of $\gamma = 0.5$ was selected based on information presented by Johnson and Elimelech (1995)). Consequently, the value of S_{max} also increases with IS in Fig. 1. It should be mentioned that more complex, non-uniform distributions of A_f may occur at the pore-scale as a result of physical and/or chemical heterogeneity that produces primary and/or secondary minimum interactions. Nevertheless, A_f and S_{max} will still be functions of IS.

Fig. 1 indicates that a reduction in IS may produce a corresponding decrease in A_f and S_{max}. This change in A_f and S_{max} induces colloid release within the area defined by A_{if}-A_f, where A_{if} [−] is the initial value of A_f before chemical alteration. The new equilibrium value of S is given as:

$$S = f_{nr} S_i \tag{5}$$

where S_i [$N\ M^{-1}$] is the initial value of S before chemical alteration, and f_{nr} [−] is the fraction of retained colloids that is not released by the chemical alteration ($f_{nr} \le 1$). Similarly, the amount of colloid release with the IS reduction is equal to $(1\text{-}f_{nr})^*S_i$. If the retained colloids are uniformly distributed within A_{if}, then the value of f_{nr} is related to A_f and S_{max} as (Bradford et al., 2012):

$$f_{nr} = \frac{A_f}{A_{if}} = \frac{S_{\max}}{S_{i\max}} \tag{6}$$

where S_{imax} [$N\ M^{-1}$] is the initial value of S_{max}. It should be mentioned that the above analysis also applies to the representative elementary area or volume scales. In this case, values of A_f and S_{max} are continuous functions of IS in Eq. (6), and S_i and S may be functions of depth in Eq. (5).

Theoretical estimates of A_f have been made for various physicochemical conditions by conducting a torque balance over an idealized porous medium surface (Bradford and Torkzaban, 2012; Bradford et al., 2013). Variations in the amount, size, and charge of nanoscale chemical heterogeneity on the solid and colloid surfaces produced localized primary minimum interactions and corresponding A_f values that

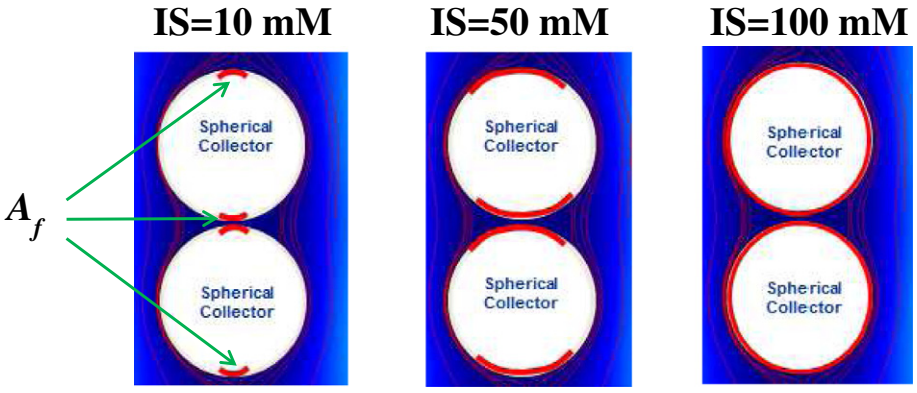

Fig. 1. An illustration of the hypothetical fraction of the solid surface area that contributes to colloid immobilization (A_f) for two spherical collectors at ionic strengths (IS) of 10, 50, and 100 mM. When IS is reduced from 100 to 50 and further to 10 mM, particles originally deposited on the "non A_f" part (white) of the collector surface tend to be released. (For interpretation of the references to color in this figure legend, the reader is referred to the web version of this article.)

changed with the IS and colloid size (Bradford and Torkzaban, 2012). In the presence of a secondary minimum, results demonstrate that A_f will depend on the IS, the zeta potential of the colloid and porous medium, q_w, the amount and size of nanoscale heterogeneity on the solid surfaces, the colloid size, and the surface roughness and pore–space geometry (Bradford et al., 2013). A potential advantage of the theoretical approach is independent model predictions for the amount of colloid release over a wide range of conditions. Furthermore, the amount of colloid release from primary and secondary minimum interactions can be explicitly quantified for a variety of solid and colloid properties. Unfortunately, a priori information on all the required nanoscale physical and chemical model parameters for the theoretical approach is still not available, and future research is still needed to overcome these limitations. Consequently, values of f_{nr} (Eq. (6)) as a function of selected physicochemical conditions were obtained directly using mass balance information (Bradford et al., 2012; Torkzaban et al., 2013) from transient release experiments discussed below. Experimental data for f_{nr} is expected to be of critical importance for calibration and validation of theoretical predictions for A_f.

3.3. Models for transient colloid release

The previous section demonstrates that the amount of colloid release due to transient physicochemical conditions can be related to changes in A_f. Furthermore, this analysis holds for colloids interacting in either a secondary or primary minimum. A second critical step in modeling colloid release with transient physicochemical conditions is accurately describing the rate of release. This issue is addressed in this section.

Eq. (1) is again used to describe colloid transport during transient physicochemical conditions. In addition, similar transport equations with associated reactions are solved for geochemical species of interest (e.g., cations, anions, and protons), and quantities such as the IS, pH, and the fraction of cation exchange sites occupied by multivalent cations (f_{++}) can be calculated. The specific number of geochemical species, transport equations, and reactions types that are needed depend on the solution chemistry and the soil properties (Mayer et al., 2002; Šimůnek and Valocchi, 2002). The travel velocity of chromatographic fronts (e.g., IS, pH, and cation exchange) approaches that of a conservative tracer for sand with a very low cation exchange capacity (Torkzaban et al., 2013).

An equilibrium expression for colloid release with a chemical perturbation can be derived from Eqs. (5) and (6) by taking the partial derivative of S with respect to time and applying the chain rule. The following equilibrium expressions apply for colloid release with changes in IS shown in Fig. 1:

$$\rho_b \frac{\partial S}{\partial t} = \rho_b \frac{S_i}{A_{if}} \frac{\partial A_f}{\partial t} H_o\left(-\frac{\partial A_f}{\partial t}\right) \tag{7a}$$

$$\begin{aligned}\rho_b \frac{\partial S}{\partial t} &= \rho_b \frac{S_i}{A_{if}} \left(\frac{dA_f}{dC_{IS}} \frac{\partial C_{IS}}{\partial t}\right) H_o\left(-\frac{\partial C_{IS}}{\partial t}\right) \\ &= \rho_b S_i \left(\frac{df_{nr}}{dC_{IS}} \frac{\partial C_{IS}}{\partial t}\right) H_o\left(-\frac{\partial C_{IS}}{\partial t}\right)\end{aligned} \tag{7b}$$

where C_{IS} is the IS of the aqueous phase (e.g., moles/liter), and H_o is a Heaviside function that is equal to 0 when $-\frac{\partial C_{IS}}{\partial t} < 0$ and 1 when $-\frac{\partial C_{IS}}{\partial t} \geq 0$ to turn release on when the IS decreases and the depth of the secondary or primary minimum is reduced. Eq. (7a) indicates that release only occurs when $\frac{\partial A_f}{\partial t} < 0$. Note that potential retention (e.g., reattachment) of released colloids is not explicitly considered in Eq. (7a) and (7b). As a first approximation we assume that subsequent retention of the released colloids during Phase 3 was negligible because chemical conditions were altered in favor of colloid release, and it is only possible to experimentally determine the net change in colloid release and retention. Significant amounts of colloid release occurred during transient physicochemical conditions (Fig. 2), whereas negligible detachment occurred under steady-state conditions (Table 2). Consequently, the value of k_{rs} was also set to zero during Phase 3.

In addition to IS, experimental information presented below indicates that A_f is also a function of pH and q_w, with colloid release initiated when the pH and q_w increases. In addition, theoretical information discussed above and experimental results (Grolimund and Borkovec, 2006; Torkzaban et al., 2013) indicate that adsorption of multivalent cations may alter the amount of nanoscale chemical heterogeneity, and that A_f may therefore be a function of f_{++}. Similar equilibrium expressions for colloid release may be derived for each of these cases as:

$$\begin{aligned}\rho_b \frac{\partial S}{\partial t} &= \rho_b \frac{S_i}{A_{if}} \left(\frac{dA_f}{dC_{pH}} \frac{\partial C_{pH}}{\partial t}\right) H_o\left(\frac{\partial C_{pH}}{\partial t}\right) \\ &= \rho_b S_i \left(\frac{df_{nr}}{dC_{pH}} \frac{\partial C_{pH}}{\partial t}\right) H_o\left(\frac{\partial C_{pH}}{\partial t}\right)\end{aligned} \tag{8}$$

$$\begin{aligned}\rho_b \frac{\partial S}{\partial t} &= \rho_b \frac{S_i}{A_{if}} \left(\frac{dA_f}{df_{++}} \frac{\partial f_{++}}{\partial t}\right) H_o\left(-\frac{\partial f_{++}}{\partial t}\right) \\ &= \rho_b S_i \left(\frac{df_{nr}}{df_{++}} \frac{\partial f_{++}}{\partial t}\right) H_o\left(-\frac{\partial f_{++}}{\partial t}\right)\end{aligned} \tag{9}$$

$$\begin{aligned}\rho_b \frac{\partial S}{\partial t} &= \rho_b \frac{S_i}{A_{if}} \left(\frac{dA_f}{dq_w} \frac{\partial q_w}{\partial t}\right) H_o\left(\frac{\partial q_w}{\partial t}\right) \\ &= \rho_b S_i \left(\frac{df_{nr}}{dq_w} \frac{\partial q_w}{\partial t}\right) H_o\left(\frac{\partial q_w}{\partial t}\right)\end{aligned} \tag{10}$$

where C_{pH} is the aqueous phase pH (e.g., $-\log_{10}(C_H)$; and C_H is moles of hydrogen ions per liter). A composite expression may also be developed for the total exchange during colloid release with changes in C_{IS}, C_{pH}, f_{++}, and q_w as:

$$\rho_b \frac{\partial S}{\partial t} = \rho_b \frac{S_i}{A_{if}} \left(\frac{dA_f}{dC_{IS}} \frac{\partial C_{IS}}{\partial t} + \frac{dA_f}{dC_{pH}} \frac{\partial C_{pH}}{\partial t} + \frac{dA_f}{df_{++}} \frac{\partial f_{++}}{\partial t} + \frac{dA_f}{dq_w} \frac{\partial q_w}{\partial t}\right) H_o\left(-\frac{\partial A_f}{\partial t}\right) \tag{11}$$

Eq. (11) indicates that transient release is proportional to the total derivative of A_f with respect to time. This equation may also be rewritten in terms of f_{nr} in a similar manner to Eqs. (7b)–(10). The determination of C_{IS}, C_{pH}, and f_{++} and their partial derivatives with respect to time in Eqs. (7b)–(11) follows directly from the solution of the geochemistry transport equations, whereas similar information for q_w is obtained from the solution of the water flow equation.

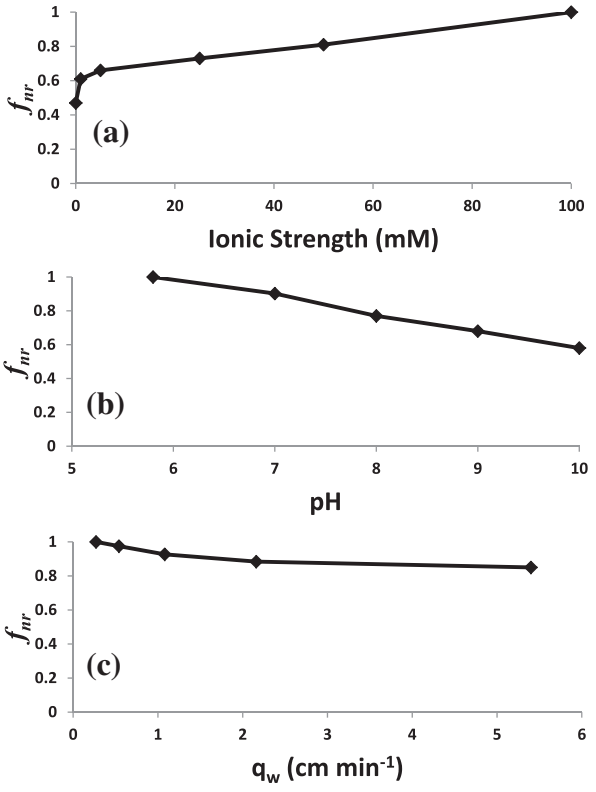

Fig. 2. Experimental values of f_{nr} as a function of IS (Fig. 2a), pH (Fig. 2b), and q_w (Fig. 2c) for *E. coli* D21g. The cells were initially deposited in 100 mM NaCl solution at pH = 5.8. The IS and pH were successively altered in a and b, respectively. In c the IS was first decreased to 5 mM, and then q_w was successively increased. Values of f_{nr} where determined from mass balance information on cell release during Phase 3.

A kinetic expression for colloid release with transients in solution chemistry that is consistent with Eqs. (5) and (6) is given as (Bradford et al., 2012):

$$\rho_b \frac{\partial S}{\partial t} = -\rho_b k_{det1}(S - f_{nr}S_i)H_o(S - f_{nr}S_i) \tag{12}$$

where k_{det1} [T^{-1}] is the transient release rate coefficient. The driving force for colloid release in this kinetic model is the difference in the actual S and the equilibrium value of S given by $f_{nr}S_i$ in Eq. (5). Recall that Eq. (6) indicates that $f_{nr} = A_f/A_{if}$, and A_f is a function of C_{IS}, C_{pH}, f_{++}, and q_w. Bradford et al. (2012) and Torkzaban et al. (2013) employed Eq. (12) to simulate the release of latex colloids, microbes, and nanoparticles under transient IS conditions and/or cation exchange.

A combined equilibrium and kinetic model for colloid release during transient conditions can also be derived using similar approaches. In this case, S is divided into equilibrium and kinetic sites, and Eq. (5) is rewritten to give the new equilibrium value as:

$$S = S_{eq} + S_{k1} = F_{eq}f_{nr}S_i + F_{k1}f_{nr}S_i \tag{13}$$

where F_{eq} [–] is the fraction of equilibrium sites, F_{k1} [–] is the fraction of kinetic sites that is equal to $F_{k1} = 1\text{-}F_{eq}$, and S_{eq} [N M^{-1}] and S_{k1} [N M^{-1}] are the equilibrium and kinetic solid phase concentrations of retained colloids, respectively. The exchange terms for equilibrium and kinetic sites follow directly from above as:

$$\rho_b \frac{\partial S_{eq}}{\partial t} = -\rho_b F_{eq}\frac{S_i}{A_{if}}\frac{\partial A_f}{\partial t}H_o\left(-\frac{\partial A_f}{\partial t}\right) \tag{14}$$

$$\rho_b \frac{\partial S_{k1}}{\partial t} = -\rho_b k_{det1}(S_{k1} - F_{k1}f_{nr}S_i)H_o(S_k - F_{k1}f_{nr}S_i) \tag{15}$$

A two-site kinetic release model can be developed in a similar manner to Eqs. (13)–(15). In this case, S is divided between the two kinetic sites to give the new equilibrium value as:

$$S = S_{k1} + S_{k2} = F_{k1}f_{nr}S_i + F_{k2}f_{nr}S_i \tag{16}$$

where the subscripts *k1* and *k2* on variables are used to denote kinetic sites 1 and 2, respectively. Release from the first kinetic site is again given by Eq. (15), whereas release for the second kinetic site is given as:

$$\rho_b \frac{\partial S_{k2}}{\partial t} = -\rho_b k_{det2}(S_{k2} - F_{k2}f_{nr}S_i)H_o(S_{k2} - F_{k2}f_{nr}S_i) \tag{17}$$

where k_{det2} [T^{-1}] is the release rate coefficient for kinetic sites 2 and $F_{k2} = 1\text{-}F_{k1}$. Similarly, S can be divided between equilibrium and two kinetic sites, and release may be simulated using Eqs. (14), (15), and (17).

The equilibrium (Eq. (11)), kinetic (Eq. (12), combined equilibrium and kinetic (Eqs. (14)–(15)), and two-site kinetic (Eqs. (17)–(18)) models have 0, 1 (k_{det1}), 2 (F_{eq}, k_{det1}), and 3 (F_{k1}, k_{det1}, k_{det2}) fitting parameters, respectively. Simulations can be quite different when using the various release model formulations. In general, release occurs very rapidly when using the equilibrium model and this approach has limited flexibility due to the lack of fitting parameters. The kinetic model can reproduce a wide range of release behaviors depending on the value of k_{det1}. When k_{det1} is high the kinetic model approaches equilibrium conditions, whereas when k_{det1} is low the kinetic model predicts slow and prolonged release. The greatest model flexibility occurs with the combined equilibrium and kinetic or two-site kinetic models because of the greater number of parameters. Variation of these parameters can produce different combinations of rapid (equilibrium) and slow kinetic release behavior. It should also be mentioned that all of the above models are proportional to S_i. Consequently, factors that promote smaller amounts of retention during

Table 2
Fitted model parameters to the colloid breakthrough curves during Phases 1 and 2. The standard error associated with the parameter fit is given in the parenthesis.

Figures	Transient	k_{sw} min^{-1}	k_{rs} min^{-1}	S_{max}/C_o cm^{3}g^{-1}	R^2
2a, 3a	IS	0.087 (0.002)	0.002 (0.000)	2.11 (0.11)	0.98
2b, 3b	pH	0.090 (0.002)	0.001 (0.000)	5.36 (0.63)	0.98
2c	q_w	0.076 (0.002)	0.002 (0.000)	4.27 (0.78)	0.96
4a	Exchange/IS	0.057 (0.001)	0.002 (0.000)	3.35 (0.48)	0.98
4b	Exchange/IS	0.195 (0.009)	0.002 (0.000)	5.03 (1.11)	0.75

Phases 1 and 2 (e.g., lower IS and influent colloid concentrations), will also produce smaller amounts of release during Phase 3.

4. Results and discussion

4.1. Amount of transient colloid release

A critical issue in the application of the above models is the determination of the functional dependency of f_{nr} (which is related to A_f and S_{max} by Eq. (6)) on solution chemistry and/or hydrodynamic parameters. In this work, values of f_{nr} were directly determined using mass balance information from the transient release experiments. Fig. 2a presents experimental values of f_{nr} as a function of IS for *E. coli* D21g when the cells were initially deposited in 100 mM NaCl solution at pH = 5.8. A decrease in IS produces a nonlinear decrease in f_{nr}, especially at lower IS. This behavior reflects successive decreases in the adhesive interaction between D21g and the porous medium. In particular, the calculated height of the energy barrier increases and the depth of the secondary minimum decreases for decreasing IS (Table 1). The final value of f_{nr} = 0.47 in DI water at pH = 5.8, which indicates that a significant amount of D21g was still retained in the sand even when the secondary minimum was eliminated. Most of the D21g can be recovered from quartz sand after excavation of the sand into excess solution of the same solution chemistry (Torkzaban et al., 2008). The nonlinearity of f_{nr} at lower IS and continued D21g retention in DI water likely reflect the effects of spatial variations in the distribution of the applied hydrodynamic and resisting adhesive torques that are discussed in Section 1.

It should also be mentioned that values of f_{nr} shown in Fig. 2 can be converted to $A_f = f_{nr}A_{if}$ using Eq. (6). In this case, Eq. (4) can be used to calculate A_{if} from values of S_{max} (Table 2) that were obtained by fitting to the breakthrough curve during Phases 1 and 2. Interestingly, the value of A_{if} was very small (<0.8–1.9%) even though the solution chemistry (100 mM NaCl and pH = 5.8) was predicted to be favorable for cell attachment (Table 1). Furthermore, DLVO theory predicts that the cells would be irreversibly retained in a primary minimum because of its infinite depth. These discrepancies can be explained by factors that are not considered in these DLVO calculations. For example, the combined influence of Born repulsion and nanoscale surface roughness has been demonstrated to produce a finite depth of the primary minimum that changes with solution IS in a similar manner to the secondary minimum (Bradford and Torkzaban, 2013; Shen et al., 2012), and some of the colloids in a primary minimum may therefore be susceptible to hydrodynamic removal (Treumann et al., 2014). Colloid release from a primary minimum during physicochemical perturbations has also been attributed to chemical heterogeneity and steric forces (Pazmino et al., 2014).

Fig. 2b presents experimental values of f_{nr} as a function of pH for *E. coli* D21g when the cells were initially deposited in 100 mM NaCl solution at pH = 5.8. An increase in pH produces almost a linear decrease in f_{nr}. Similar to the IS data, these changes reflect successive decreases in the mean adhesive interaction. An increase in solution pH tends to produce a decrease in the zeta potentials (more negative) for D21g and the sand that make conditions less favorable for attachment. However, strong primary or deep secondary minima (<− 19.6 kT) were predicted for all of these pH conditions because of the high IS conditions (Table 1). Consequently, these DLVO calculations cannot explain the observed release behavior. The DLVO calculations employed macroscopic values of zeta potentials, and therefore do not account for the influence of nanoscale chemical heterogeneity on interaction energies. Nanoscale chemical heterogeneity can have a large influence on the mean and variance of the interaction energy (Bendersky and Davis, 2011; Bradford and Torkzaban, 2013). Consequently, the observed sensitivity of f_{nr} to pH implies that the amount or charge of the chemical heterogeneity is decreasing with an increase in solution pH due to deprotonation of positively or neutrally charged sites. The presence of nanoscale chemical heterogeneity may also explain some of the cell retention in DI (Fig. 2a). However, the final value of f_{nr} = 0.58 in 100 mM NaCl solution at pH = 10, and this indicates that nanoscale chemical heterogeneity cannot explain most of the D21g retention.

Additional experiments were conducted to examine the influence of q_w on D21g release. In this case, D21g was deposited in 100 mM NaCl at pH 5.8 (Phases 1 and 2), and then the IS was reduced to 5 mM NaCl (Phase 3). The value of q_w was then sequentially increased from 0.27 to 5.4 cm min^{-1} (Phase 3). Fig. 2c presents experimental values of f_{nr} as a function of q_w for D21g when the IS = 5 mM NaCl. Little D21g release was observed with increases in q_w. Some researchers have noted a similar insensitivity of colloid release to increasing q_w (Johnson et al., 2010), whereas others have shown a greater dependency of colloid release on q_w (Bergendahl and Grasso, 1998, 2000). These differences can likely be explained by differences in the adhesive interaction, the hydrodynamic conditions, and the locations for retention. In particular, the effects of q_w are expected to increase when the resisting adhesive torque is smaller (e.g., lower IS and/or higher pH). Furthermore, the applied hydrodynamic torque increases with the cube of the colloid radius, and also increases in finer textured media (Torkzaban et al., 2007). Larger scale roughness locations and grain–grain contact points will dramatically increase the resisting adhesive torque and decrease the applied hydrodynamic torque at these locations in comparison to smooth surfaces (Bradford et al., 2013; Burdick et al., 2005). Both of these factors will tend to diminish the role of q_w on release.

4.2. Simulated colloid release

The developed models are used in this section to simulate colloid release during transient solution chemistry conditions. We did not attempt to simulate the colloid release behavior with increases in q_w (Fig. 2c) because only small amounts of colloid release occurred which were near the analytic detection limit. The initial conditions for these simulations were determined by fitting steady-state retention and release model parameters (k_{sw}, k_{rs}, and S_{max}/C_o) to breakthrough curve data for Phases 1 and 2. These model parameters are provided in Table 2, along with the Pearson correlation coefficient (R^2) for the goodness of model fit. The dispersivity ($\lambda = D/v$; where v is the pore water velocity) was set equal to 0.1 cm for all experiments based on published tracer results (Wang et al., 2013), and preliminary optimization results during Phases 1, 2, and 3. Fitted release model parameters during Phase 3 are provided in Table 3, along with R^2 and the

Table 3
Model parameters for the colloid release curve during Phase 3. The standard error is given in the parenthesis.

Fig.	Transient	Model	k_{det1} min^{-1}	k_{det2} min^{-1}	F_{eq}	F_{k1}	F_{k2}	R^2	AIC
4a	IS	E	NA	NA	1.0	NA	NA	0.54	NA
4a	IS	K	0.395 (0.064)	NA	NA	1.00	NA	0.78	−631
4a	IS	EK	0.420 (0.115)	NA	0.01 (0.19)	0.99	0.00	0.78	−628
4a	IS	2 K	0.063 (1.450)	0.391 (0.144)	NA	0.01 (0.30)	0.99	0.78	−626
4b	pH	E	NA	NA	1.0	NA	NA	0.25	NA
4b	pH	K	0.027 (0.002)	NA	NA	1.00	NA	0.47	−963
4b	pH	EK	0.023 (0.002)	NA	0.10 (0.01)	0.90	NA	0.60	−1007
4b	pH	2 K	0.019 (0.003)	0.392 (0.118)	NA	0.84 (0.03)	0.16	0.65	−1017
5a	Ex./IS	K	1.000 (0.275)	NA	NA	1.00	NA	0.94	−429
5b	Ex./IS	K	0.192 (0.008)	NA	NA	1.00	NA	0.95	−552

NA — denotes not applicable.
Ex. — denotes cation exchange.
E — denotes equilibrium model.
K — denotes kinetic model.
EK — denotes equilibrium and kinetic model.
2K — denotes 2 site kinetic model.

Akaike information criterion (AIC) (Akaike, 1974) for the goodness of model fit. The AIC value was determined as:

$$AIC = n\log\left(\sigma^2\right) + 2k + \frac{2k(k+1)}{n-k-1} \quad (18)$$

where n [–] is the number of observations, σ^2 [–] is the residual variance estimated as the sum of squared residuals divided by n, and k [–] is the number of estimated parameters. The value of R^2 tends to increase with the number of model fitting parameters. Conversely, the AIC is a measure of the goodness of fit that penalizes for adding fitting parameters. The model that produces that best description of the data with the smallest number of fitting parameters (the lowest AIC) is preferred.

Fig. 3 presents observed D21g breakthrough and release curves with changes in IS (Fig. 3a) and pH (Fig. 3b). Simulated changes in the solution composition (IS or pH) are also shown in these figures. The final reduction in solution IS from 1 mM to DI water is difficult to see in Fig. 3a, but it occurs after around 420 min. The release curves were simulated using the various model formulations and the model result with the lowest AIC is shown in the figure. Release model parameters and AIC information provide valuable information on the rates of colloid release and the most appropriate model formulation under the considered physicochemical conditions, respectively. Values of AIC indicate that the one-site kinetic model was preferred for D21g release with changes in solution IS, and that the agreement between the model and data was reasonable (Table 3). The fitted value of k_{det1} was high (k_{det1} = 0.395 min^{-1}). This implies that colloid release and changes in the mean adhesive interaction (primary or secondary minimum) with IS reduction (Table 1) occurred very rapidly and approached equilibrium conditions. In contrast, AIC values indicated that the two-site kinetic model was best to describe release with changes in solution pH and that it provided a reasonable characterization of the data (Table 3). The first kinetic site exhibited a slow rate of colloid release (k_{det1} = 0.019 min^{-1}), whereas the second kinetic site produced a much more rapid rate of release (k_{det2} = 0.392 min^{-1}). The rapid colloid release behavior likely reflects changes in the mean adhesive interaction (Table 1) in a manner similar to IS reduction (Fig. 3a). Conversely, the slow colloid release likely is associated with alteration of nanoscale chemical heterogeneity by deprotonation of hydroxyl sites as the pH increases. Most of the initial colloid mass was associated with this slow rate of colloid release (F_{k1} = 0.84).

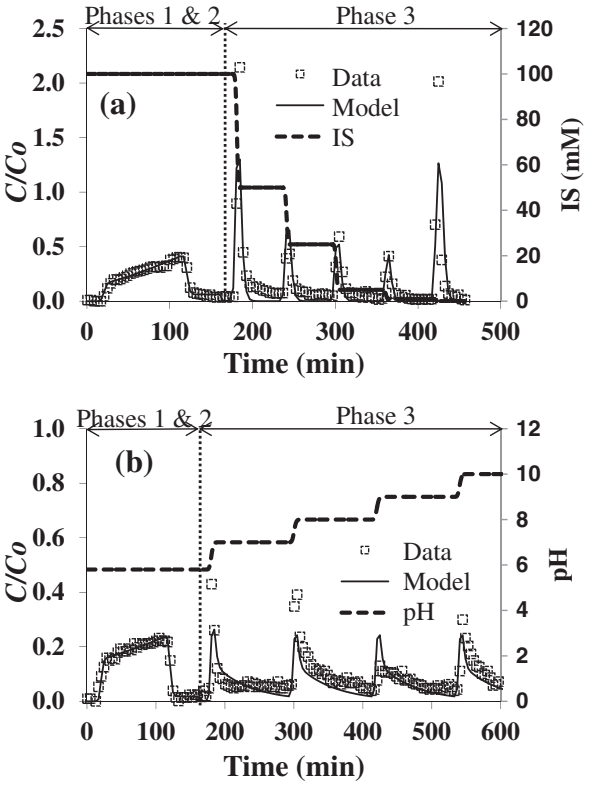

Fig. 3. Observed and simulated breakthrough and release curves for D21g with changes of IS (a) and pH (b) using experimental values of f_{nr} shown in Fig. 2. Cells were initially deposited in 100 mM NaCl at pH 5.8 (Phases 1 and 2), then the IS (100, 50, 25, 5, 1, and 0 mM) or pH (5.8, 7, 8, 9, and 10) was sequentially changed during Phase 3. The value of q_w was 0.276 cm min^{-1}. The 1 site kinetic model was used in (a), and the 2 site kinetic model was used in (b). Model parameters are given in Tables 2 and 3.

Fig. 4 presents observed and simulated values of D21g (Fig. 4a) and CML NP (Fig. 4b) breakthrough and release curves when employing the following solution chemistry sequence: deposition in 2 mM $CaCl_2$ solution (Phase 1); eluting in 2 mM $CaCl_2$ solution (Phase 2); flushing with DI water (Phase 3a); flushing with 100 mM NaCl solution (Phase 3b); and flushing with DI water (Phase 3c). Note that there are drastic differences in the amount of D21g and CML NP retention and release for this solution chemistry sequence. In particular, greater amounts of retention occurred for CML NPs than D21g in 2 mM $CaCl_2$ solution. Traditional DLVO calculations cannot explain this difference because the secondary minimum is greater for D21g than CML NPs and the energy barrier is sufficiently high to eliminate most primary minima interactions (Table 1). Release of D21g mainly occurred in the first DI water pulse (Phase 3a). Conversely, release of CML NPs mainly occurred with the second DI water pulse (Phase 3c).

Nanoscale chemical heterogeneity provides one plausible explanation for the differences in D21g and CML NP retention and release shown in Fig. 4. In particular, surface integration calculations demonstrate that nanoscale chemical heterogeneity can produce strong primary minima interactions for smaller colloids, whereas larger colloids will continue to mainly interact in a weak secondary minimum (Bendersky and Davis, 2011; Duffadar and Davis, 2007). Greater retention of CML NPs than D21g is therefore expected during Phases 1 and 2 due to nanoscale chemical heterogeneity created by adsorbed Ca^{2+} (Grosberg et al., 2002). The greatest amount of D21g release occurred with the first DI water pulse (Phase 3a) when the secondary minimum was eliminated. Conversely, the greatest amount of CML NP release occurred with the second DI water pulse (Phase 3c). This difference in release with DI water for D21g and CML NPs is also due to differences in the sensitivity of D21g and CML NPs to chemical heterogeneity. Addition of 100 mM NaCl (Phase 3b) initiates cation exchange (data not shown) that likely converts some of the primary to secondary minima interactions for CML NPs but not for D21g. Values of f_{nr} for CML NPs were therefore lower for the second than the first DI water pulse.

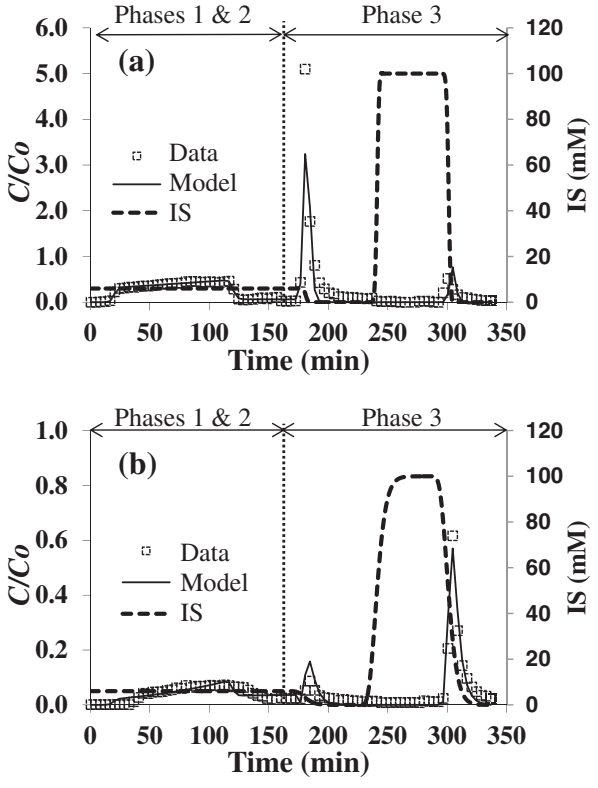

Fig. 4. Observed and simulated breakthrough and release curves for D21g (a) and 20 nm CML NPs (b) when employing the following solution chemistry sequence: deposition in 2 mM $CaCl_2$ solution (Phase 1); eluting in 2 mM $CaCl_2$ solution (Phase 2); flushing with DI water (Phase 3a); flushing with 100 mM NaCl solution (Phase 3b); and flushing with DI water (Phase 3c). The simulations employed values of f_{nr} that were directly obtained from this experimental balance information and by fitted release parameters given in Table 3.

Others have similarly observed that the release of clay, coliphage, and nanoparticles was sensitive to the processes of cation exchange (Grolimund and Borkovec, 2006; Sadeghi et al., 2013) or the sequence of cation exchange and IS reduction (Bradford and Kim, 2010; Torkzaban et al., 2013). Fig. 4 indicates that D21g and CML NP release was not directly initiated by decreasing f_{++} (e.g., cation exchange during Phase 3b). This implies that A_f was mainly a function of IS, but that this dependency on IS was altered by a decrease in the amount of adsorbed Ca^{2+} (Phase 3b), especially for the smaller CML NPs. Similar to release with a reduction of IS shown in Fig. 3a, the release behavior of D21g and CML NPs occurred very rapidly and approached equilibrium conditions that were reasonably described by the one-site kinetic model (Table 3). Additional research is needed to better resolve the dependence of A_f on f_{++} and IS.

5. Summary and conclusions

Two fundamental issues must be resolved in order to simulate colloid release with transient physicochemical conditions. One challenge is determining the amount of colloid release with a given perturbation. In this work, we relate the amount of transient colloid release to changes in the fraction of the solid surface area that contributes to colloid retention (A_f). Functional relations between A_f and selected physicochemical conditions may be determined from experimental mass balance information or estimated theoretically. A second challenge is modeling the rates of colloid release. We develop equilibrium, kinetic, and combined equilibrium and kinetic models to describe various colloid release behavior with changes in A_f. Our approach is quite general and is applicable to colloid release initiated by alteration of mean and/or local (nanoscale heterogeneity) adhesive interactions (secondary or primary minima), as well as hydrodynamic forces.

Column transport and release experiments were conducted to study the release behavior of *E. coli* D21g and CML NPs under different physicochemical conditions, to determine A_f relations, and to test the ability of the developed models to describe this data. Release of *E. coli* D21g from a primary minimum was promoted by a decrease in solution IS, similar to expected trends for a secondary minimum. However, a large fraction of the D21g was still retained in the sand even when the secondary minimum was eliminated, suggesting the important role of macroscopic surface roughness and grain–grain contacts on cell retention. Cell release was also promoted by increases

in solution pH even though strong primary or secondary minimum were predicted. This observation suggested that a reduction in nanoscale chemical heterogeneity with an increase in pH also contributed to cell release. In contrast to D21g, release of CML NPs that were initially deposited in the presence of 2 mM $CaCl_2$ solution occurred only after exchange of Ca^{2+} by Na^{+} and then a reduction in the solution IS. These observations suggest that reversible primary minimum interactions can occur for colloids on solid surfaces due to factors such as non-DLVO forces and nanoscale physical and chemical heterogeneity. Temporal changes in the water velocity did not have a large influence on the release of D21g. This insensitivity was likely due to factors that reduce the applied hydrodynamic torque and/or increase the resisting adhesive torque; e.g., large-scale roughness locations and grain–grain contacts.

The developed models provided a reasonable description of the colloid release when parameters were optimized to the experimental data. However, the required complexity of the release model depended on the specific transient condition. For example, D21g release with changes in IS was well described with a one-site kinetic model that approached equilibrium conditions. This implies that changes in the mean adhesive interaction (primary or secondary minimum) with IS reduction occurred very rapidly. In contrast, D21g release with changes in pH was better quantified with a two-site kinetic model, with most of the colloid release occurring slowly and only a small fraction rapidly. The rapid colloid release likely reflects changes in the mean adhesive interaction in a similar manner to the IS data. The slow colloid release presumably occurred due to alteration of nanoscale chemical heterogeneity by deprotonation of hydroxyl sites as the pH increases.

Acknowledgments

This research was supported by the 214 Manure and Byproduct Utilization Project of the USDA-ARS. Mention of trade names and company names in this manuscript does not imply any endorsement or preferential treatment by the USDA. We would also like to acknowledge the help of Dr. Brendan Headd in conducting these transport and release experiments.

References

Adamczyk, Z., Siwek, B., Zembala, M., 1992. Reversible and irreversible adsorption of particles on homogeneous surfaces. Colloids Surf. 62, 119–130.
Adamczyk, Z., Siwek, B., Zembala, M., Belouschek, P., 1994. Kinetics of localized adsorption of colloid particles. Adv. Colloid Interf. Sci. 48, 151–280.
Adamczyk, Z., Siwek, B., Szyk, L., 1995. Flow-induced surface blocking effects in adsorption of colloid particles. J. Colloid Interface Sci. 174, 130–141.
Akaike, H., 1974. A new look at statistical model identification. IEEE Trans. Autom. Control 19, 716–722.
Bedrikovetsky, P., Siqueira, F.D., Furtado, C.A., Souza, A.L.S., 2011. Modified particle detachment model for colloidal transport in porous media. Transp. Porous Media 86, 353–383.
Bendersky, M., Davis, J.M., 2011. DLVO interaction of colloidal particles with topographically and chemically heterogeneous surfaces. J. Colloid Interface Sci. 353, 87–97.
Bergendahl, J., Grasso, D., 1998. Colloid generation during batch leaching tests: mechanics of disaggregation. Colloids Surf. A Physicochem. Eng. Asp. 135, 193–205.
Bergendahl, J., Grasso, D., 1999. Prediction of colloid detachment in a model porous media: thermodynamics. AICHE J. 45, 475–484.
Bergendahl, J., Grasso, D., 2000. Prediction of colloid detachment in a model porous media: hydrodynamics. Chem. Eng. Sci. 55, 1523–1532.
Bradford, S.A., Kim, H., 2010. Implications of cation exchange on clay release and colloid-facilitated transport in porous media. J. Environ. Qual. 39, 2040–2046.
Bradford, S.A., Kim, H., 2012. Causes and implications of colloid and microorganism retention hysteresis. J. Contam. Hydrol. 138–139, 83–92.
Bradford, S.A., Torkzaban, S., 2012. Colloid adhesive parameters for chemically heterogeneous porous media. Langmuir 28, 13643–13651.
Bradford, S.A., Torkzaban, S., 2013. Colloid interaction energies for physically and chemically heterogeneous porous media. Langmuir 29, 3668–3676.
Bradford, S.A., Kim, H., Haznedaroglu, B.Z., Torkzaban, S., Walker, S.L., 2009. Coupled factors influencing concentration-dependent colloid transport and retention in saturated porous media. Environ. Sci. Technol. 43, 6996–7002.
Bradford, S.A., Torkzaban, S., Wiegmann, A., 2011. Pore-scale simulations to determine the applied hydrodynamic torque and colloid immobilization. Vadose Zone J. 10, 252–261.
Bradford, S.A., Torkzaban, S., Kim, H., Simunek, J., 2012. Modeling colloid and microorganism transport and release with transients in solution ionic strength. Water Resour. Res. 48, W09509. http://dx.doi.org/10.1029/2012WR012468.
Bradford, S.A., Torkzaban, S., Shapiro, A., 2013. A theoretical analysis of colloid attachment and straining in chemically heterogeneous porous media. Langmuir 29, 6944-2952.
Burdick, G.M., Berman, N.S., Beaudoin, S.P., 2005. Hydrodynamic particle removal from surfaces. Thin Solid Films 488, 116–123.
Delory, G.E., King, E.J., 1945. A sodium carbonate–bicarbonate buffer for alkaline phosphatases. Biochem. J. 39, 245-245.
Derjaguin, B.V., Landau, L.D., 1941. Theory of the stability of strongly charged lyophobic sols and of the adhesion of strongly charged particles in solutions of electrolytes. Acta Physicochim. U.S.S.R. 14, 733–762.
Duffadar, R.D., Davis, J.M., 2007. Interaction of micrometer-scale particles with nanotextured surfaces in shear flow. J. Colloid Interface Sci. 308, 20–29.
Elimelech, M., Gregory, J., Jia, X., Williams, R.A., 1995. Particle Deposition and Aggregation: Measurement, Modeling, and Simulation. Butterworth-Heinemann, Oxford, England.
Gregory, J., 1981. Approximate expression for retarded van der Waals interaction. J. Colloid Interface Sci. 83, 138–145.
Grolimund, D., Borkovec, M., 2006. Release of colloidal particles in natural porous media by monovalent and divalent cations. J. Contam. Hydrol. 87, 155–175.
Grolimund, D., Barmettler, K., Borkovec, M., 2001. Release and transport of colloidal particles in natural porous media 2. Experimental results and effects of ligands. Water Resour. Res. 37, 571–582.
Grosberg, A.Y., Nguyen, T.T., Shklovskii, B.I., 2002. Colloquium: the physics of charge inversion in chemical and biological systems. Rev. Mod. Phys. 74, 329.
Hogg, R., Healy, T.W., Fuerstenau, D.W., 1966. Mutual coagulation of colloidal dispersions. Trans. Faraday Soc. 62, 1638–1651.
Johnson, P.R., Elimelech, M., 1995. Dynamics of colloid deposition in porous media: blocking based on random sequential adsorption. Langmuir 11, 801–812.
Johnson, W.P., Pazmino, E., Ma, H., 2010. Direct observations of colloid retention in granular media in the presence of energy barriers, and implications for inferred mechanisms from indirect observations. Water Res. 44, 1158–1169.
Khilar, K.C., Fogler, H.S., 1984. The existence of a critical salt concentration for particle release. J. Colloid Interface Sci. 101, 214–224.
Lenhart, J.J., Saiers, J.E., 2003. Colloid mobilization in water-saturated porous media under transient chemical conditions. Environ. Sci. Technol. 37, 2780–2787.
Mayer, K.U., Frind, E.O., Blowes, D.W., 2002. Multicomponent reactive transport modeling in variably saturated porous media using a generalized formulation for kinetically controlled reactions. Water Resour. Res. 38, 1174. http://dx.doi.org/10.1029/2001WR000862.
Pazmino, E., Trauscht, J., Johnson, W.P., 2014. Release of colloids from primary minimum contact under unfavorable conditions by perturbations in ionic strength and flow rate. Environ. Sci. Technol. 48, 9227–9235.
Rijnaarts, H.H.M., Norde, W., Bouwer, E.J., Lyklema, J., Zehnder, A.J.B., 1995. Reversibility and mechanism of bacterial adhesion. Colloids Surf. B 4, 5–22.
Roy, S.B., Dzombak, D.A., 1996. Colloid release and transport processes in natural and model porous media. Colloids Surf. A Physicochem. Eng. Asp. 107, 245–262.
Ryan, J.N., Elimelech, M., 1996. Colloid mobilization and transport in groundwater. Colloids Surf. A Physicochem. Eng. Asp. 107, 1–56.
Ryan, J.N., Gschwend, P.M., 1994. Effects of ionic-strength and flow-rate on colloid release — relating kinetics to intersurface potential-energy. J. Colloid Interface Sci. 164, 21–34.
Sadeghi, G., Behrends, T., Schijven, J.F., Hassanizadeh, S.M., 2013. Effect of dissolved calcium on the removal of bacteriophage PRD1 during soil passage: The role of double-layer interactions. J. Contam. Hydrol. 144, 78–87.
Sasidharan, S., Torkzaban, S., Bradford, S.A., Dillon, P.J., Cook, P.G., 2014. Coupled effects of hydrodynamic and solution chemistry on long-term nanoparticle

transport and deposition in saturated porous media. Colloids Surf. A Physicochem. Eng. Asp. 457, 169–179.
Shen, C., Li, B., Huang, Y., Jin, Y., 2007. Kinetics of coupled primary- and secondary-minimum deposition of colloids under unfavorable chemical conditions. Environ. Sci. Technol. 41, 6976–6982.
Shen, C., Lazouskaya, V., Zhang, H., Wang, F., Li, B., Jin, Y., Huang, Y., 2012. Theoretical and experimental investigation of detachment of colloids from rough collector surfaces. Colloids Surf. A Physicochem. Eng. Asp. 410, 98–110.
Simoni, S.F., Harms, H., Bosma, T.N.P., Zehnder, A.J.B., 1998. Population heterogeneity affects transport of bacteria through sand columns at low flow rates. Environ. Sci. Technol. 32, 2100–2105.
Šimůnek, J., Valocchi, A.J., 2002. Geochemical Transport. In: Dane, J.H., Topp, G.C. (Eds.), Methods of Soil Analysis, Part 4, Physical Methods, Third edition SSSA, Madison, WI, pp. 1511–1536 (Chapter 6.9).
Šimůnek, J., van Genuchten, M.Th., Šejna, M., 2008. Development and applications of the HYDRUS and STANMOD software packages and related codes. Vadose Zone J. 7, 587–600. http://dx.doi.org/10.2136/VZJ2007.0077 (Special Issue "Vadose Zone Modeling").
Suresh, L., Walz, J.Y., 1996. Effect of surface roughness on the interaction energy between a colloidal sphere and a flat plate. J. Colloid Interface Sci. 183, 199–213.
Torkzaban, S., Bradford, S.A., Walker, S.L., 2007. Resolving the coupled effects of hydrodynamics and DLVO forces on colloid attachment to porous media. Langmuir 23, 9652–9660.
Torkzaban, S., Tazehkand, S.S., Walker, S.L., Bradford, S.A., 2008. Transport and fate of bacteria in porous media: coupled effects of chemical conditions and pore space geometry. Water Resour. Res. 44, W04403. http://dx.doi.org/10.1029/2007WR006541.
Torkzaban, S., Bradford, S.A., Wan, J., Tukunaga, T., Masoudih, A., 2013. Release of quantum dot nanoparticles in porous media: role of cation exchange and aging time. Environ. Sci. Technol. 47, 11528–11536.
Tosco, T., Tiraferri, A., Sethi, R., 2009. Ionic strength dependent transport of microparticles in saturated porous media: modeling mobilization and immobilization phenomena under transient chemical conditions. Environ. Sci. Technol. 43, 4425–4431.
Treumann, S., Torkzaban, S., Bradford, S.A., Visalakshan, R.M., Page, D., 2014. An explanation for differences in the process of colloid adsorption in batch and column studies. J. Contam. Hydrol. 164, 219–229.
Tufenkji, N., Elimelech, M., 2005. Breakdown of colloid filtration theory: role of the secondary energy minimum and surface charge heterogeneities. Langmuir 21, 841–852.
Vaidyanathan, R., Tien, C., 1991. Hydrosol deposition in granular media under unfavorable surface conditions. Chem. Eng. Sci. 46, 967–983.
Verwey, E.J.W., Overbeek, J.Th.G., 1948. Theory of the Stability of Lyophobic Colloids. Elsevier, Amsterdam.
Waentig, L., Roos, P.H., Jakubowski, N., 2009. Labelling of antibodies and detection by laser ablation inductively coupled plasma mass spectrometry. Part III. Optimization of antibody labelling for application in a Western blot procedure. J. Anal. At. Spectrom. 24, 924–933.
Wang, Y., Bradford, S.A., Simunek, J., 2013. Transport and fate of microorganisms in soils with preferential flow under different solution chemistry conditions. Water Resour. Res. 49, 2424–2436.